

Influence of Particle Surface Area Concentration on the Production of Organic Particulate Matter in a Continuously Mixed Flow Reactor

Yuemei Han,^{*,†,§,||} Zhaoheng Gong,^{†,||} Pengfei Liu,^{†,||} Suzane S. de Sá,[†] Karena A. McKinney,^{†,‡} and Scot T. Martin^{*,†,||}

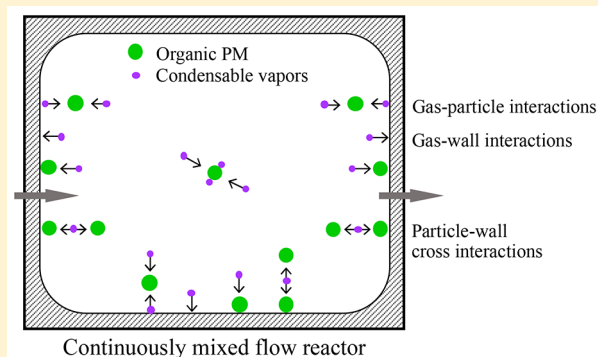
[†]School of Engineering and Applied Sciences, Harvard University, Cambridge, Massachusetts 02138, United States

[§]Key Laboratory of Aerosol Chemistry and Physics, State Key Laboratory of Loess and Quaternary Geology, Institute of Earth Environment, Chinese Academy of Science, Xi'an, Shaanxi 710061, China

^{||}Department of Earth and Planetary Sciences, Harvard University, Cambridge, Massachusetts 02138, United States

Supporting Information

ABSTRACT: Organic particulate matter (PM) was produced at different particle surface area concentrations S in a continuously mixed flow reactor (CMFR). The apparent PM yield from the dark ozonolysis of α -pinene increased from $24.5 \pm 0.7\%$ to $57.1 \pm 0.6\%$ for an increase in S from 0.55 to $2.87 \times 10^3 \mu\text{m}^2\text{-surface cm}^{-3}$ volume. The apparent yield saturated for $S > 2.1 \times 10^3 \mu\text{m}^2 \text{cm}^{-3}$. There was hysteresis in the apparent yield for experiments of increasing compared to decreasing S . The relative timescales of gas-particle interactions, gas-wall interactions, and thereby particle-wall cross interactions could explain the results. The PM carbon oxidation state and oxygen-to-carbon atomic ratio decreased from -0.19 to -0.47 and 0.62 to 0.51 , respectively, for increasing S , suggesting that greater partitioning of semivolatile organic species into the PM contributed to the increased PM yield. A thorough understanding of the role of gas-wall interactions on apparent PM yield is essential for the extension of laboratory results into predictions of atmospheric PM production, and comparative results from CMFRs and batch reactors can be informative in this regard.



1. INTRODUCTION

Laboratory studies, together with field observations and modeling simulations, constitute a comprehensive approach for understanding atmospheric chemistry and its environmental impacts.^{1,2} Environmental chambers have been widely used in laboratory investigations of atmospheric gas-phase chemistry and the production and evolution of secondary organic aerosol.^{3–7} In particular, the yield of organic particulate matter (PM) from the oxidation of volatile organic compounds (VOCs) is an important parameter derived from chamber experiments.^{8,9} These yields have been incorporated extensively into chemical transport models for the prediction of atmospheric PM production.^{10,11} Recent studies, however, suggest that many apparent yields reported in the historic literature might be lower limits instead of best estimates because of the deposition and ultimate absorption of low-volatility and semivolatile gas-phase species to the walls of Teflon bags typically used in chamber design.^{12–14}

PM yield depends largely on experimental conditions and chamber properties. The apparent PM yield is based on the produced PM mass concentration compared to the consumed VOC mass concentration. The effects of gas-wall interactions are illustrated by the dependence of PM yield on the surface area concentration of a pre-existing particle population (i.e., seed

particles).^{14–16} A competition takes place between the mass flux of condensable organic vapors to the surfaces of the pre-existing particles and the mass flux to the Teflon bag walls. Thus, far, experiments have primarily employed batch-mode chambers. In this mode, reactive VOCs and a pre-existing population of inert particles are initially introduced as a bolus into the chamber, and the VOCs are subsequently oxidized to produce PM.

An alternative mode is to operate the chamber as a continuously mixed flow reactor (CMFR).^{13,17–19} Experiments reported in the literature do not provide a systematic investigation of how the apparent PM yield depends on particle surface area concentration in a CMFR. The gas-wall deposition in medium and large-scale CMFRs with Teflon bags remains unclear, although wall effect of a small CMFR has been demonstrated to be negligible partly due to the relatively fast continuous flow in the potential aerosol mass reactor.²⁰ Complementary differences to batch chambers and hence new insights might be expected by CMFR studies. Certain semivolatile species might establish a dynamic equilibrium

Received: December 27, 2018

Revised: March 26, 2019

Accepted: March 29, 2019

Published: March 29, 2019

Table 1. Experimental Conditions and Apparent PM Yields for Different Particle Surface Area Concentrations^a

| exp. | sheath-to-aerosol flow ratio | CMFR outflow | | | |
|------|------------------------------|---|---|--|---|
| | | number concentration, N (10^3 cm^{-3}) | surface area concentration, S ($10^3 \mu\text{m}^2 \text{ cm}^{-3}$) | mass concentration, M_{org} ($\mu\text{g m}^{-3}$) | apparent yield, Y_{org} (%) |
| I-1 | na | 4.5 ± 0.3 | 0.55 ± 0.03 | 30.5 ± 0.6 | 24.5 ± 0.7 |
| I-2 | 10:1.5 | 4.4 ± 0.2 | 0.60 ± 0.02 | 32.9 ± 1.0 | 26.4 ± 1.0 |
| I-3 | 10:1.8 | 6.0 ± 0.1 | 0.78 ± 0.02 | 44.1 ± 0.7 | 35.4 ± 0.8 |
| I-4 | 10:2.1 | 10.3 ± 0.2 | 0.98 ± 0.02 | 48.2 ± 0.7 | 38.7 ± 0.8 |
| I-5 | 10:2.4 | 17.4 ± 0.3 | 1.39 ± 0.02 | 61.1 ± 0.8 | 49.0 ± 0.9 |
| I-6 | 10:2.7 | 24.1 ± 0.5 | 1.65 ± 0.03 | 65.0 ± 0.7 | 52.1 ± 0.7 |
| I-7 | 10:3.0 | 33.4 ± 0.8 | 2.06 ± 0.05 | 70.1 ± 0.7 | 56.3 ± 0.8 |
| II-1 | 10:3.3 | 49.2 ± 0.9 | 2.87 ± 0.04 | 71.2 ± 0.5 | 57.1 ± 0.6 |
| II-2 | 10:2.5 | 34.2 ± 0.3 | 2.08 ± 0.01 | 71.5 ± 0.7 | 57.4 ± 0.8 |
| II-3 | 10:2.2 | 20.1 ± 0.3 | 1.52 ± 0.02 | 70.6 ± 0.7 | 56.7 ± 0.8 |
| II-4 | 10:1.9 | 8.2 ± 0.3 | 0.93 ± 0.01 | 59.6 ± 0.9 | 47.8 ± 1.0 |
| II-5 | 10:1.6 | 5.9 ± 0.2 | 0.85 ± 0.01 | 52.8 ± 0.8 | 42.4 ± 0.9 |
| II-6 | 10:1.3 | 4.2 ± 0.1 | 0.60 ± 0.01 | 45.8 ± 0.9 | 36.8 ± 1.0 |
| II-7 | n/a | 4.3 ± 0.1 | 0.58 ± 0.01 | 44.3 ± 1.0 | 35.6 ± 1.1 |

^aSheath-to-aerosol flow ratio, particle number concentration N , particle surface area concentration S , and PM mass concentration M_{org} and apparent PM yield Y_{org} are listed. Sets I and II represent experiment series for increasing and decreasing S , respectively. Listed M_{org} and Y_{org} are corrected for particle-wall loss, as described in the main text. Conditions: 22.0 °C, 40% RH, 22 ppb ($125 \mu\text{g m}^{-3}$) α -pinene prior to ozonolysis, and 300 ppb ozone. For “n/a” in sheath-to-aerosol flow ratio, these experiments were conducted in the absence of ammonium sulfate particles.

between suspended PM and organic material deposited to the Teflon walls to achieve steady-state conditions in the CMFR. The partitioning of these product molecules between particles and bag walls could thus be different between batch-mode chambers and CMFRs, thereby altering the apparent PM yield in the two reactor configurations. For instance, higher yields were reported for α -pinene ozonolysis in a CMFR than in batch-mode chambers.⁵

Herein, the influence of particle surface area concentration S ($\mu\text{m}^2 \cdot \text{surface cm}^{-3} \cdot \text{volume}$) on PM yield and characteristics is studied for α -pinene ozonolysis in a CMFR. Comparative experiments were conducted for increasing and decreasing S . Hysteresis between the experiments is analyzed in the context of gas-particle interactions, gas-wall interactions, and thereby particle-wall cross interactions. Changes in PM composition and oxidation state with S are also examined by mass spectrometry.

2. EXPERIMENTAL METHODS

Organic particulate matter was produced by the dark ozonolysis of α -pinene in the Harvard Environmental Chamber (HEC).^{5,6,19} The HEC was operated as a CMFR during a 20 day experimental campaign. It consisted of a Teflon bag (Welch Fluorocarbon Inc.) enclosed in a temperature-controlled room. The cubic bag had a volume of 4.7 m³, and the ratio of the bag surface area to its volume was 3.6 m⁻¹. The bag was made from perfluoroalkoxy alkanes (PFA), which can be represented as chains of $-(\text{CF}_2\text{CF}_2)_n(\text{CF}_2\text{CF}(\text{OCF}_3))_m-$. Prior to the experimental campaign, the bag was vigorously oxidized to remove organic material by exposure to 300 ppb O₃ at 40 °C for 4 days, followed by flushing with zero air at 22 °C for 7 days. The temperature and relative humidity (RH) inside the bag were 22.0 ± 0.03 °C and 40.0 ± 0.4%, respectively, during the experiments. The constant RH was maintained by injecting humidified air using a feedback control system. The stated uncertainties represent precision rather than accuracy. Flows of α -pinene, ammonium sulfate particles, and ozone entered the CMFR.⁵ Steady-state conditions were obtained after a spin-up time of 12 h, corresponding to 2.7 multiples of the CMFR

residence time (4.5 h). Individual experiments were conducted in variable duration from 20 to 43 h, and observations from the last 6 h of measurements were used in the analysis. The PM in the outflow of the CMFR was sampled by instrumentation to characterize its number-diameter distribution and its chemical composition. An Aerodyne high-resolution time-of-flight aerosol mass spectrometer (HR-ToF-AMS, abbreviated AMS hereafter) was used to collect the main data sets presented herein.²¹ A collection efficiency of unity was applied for the AMS data processing (Figure S1). Further details on the experimental methods are provided in the Supporting Information (SI) (Section S1).

3. RESULTS AND DISCUSSION

3.1. Dependence of Yield on Surface Area Concentration. In a first set of experiments (labeled “I”; Table 1), the surface area concentration of the ammonium sulfate particle population was stepwise increased by adjusting the sheath-to-aerosol flow ratio (SI, Section S1). After the chamber came to steady state, the outflow S was substantially increased because of the condensation of organic material. At steady state, the outflow concentrations represented the in-chamber particle population undergoing dynamic condensational growth. The analysis herein for the dependence of yield on S is thus based on the outflow S , representing a population of organic particles having ammonium sulfate inclusions, rather than the inflow surface area concentration of the ammonium sulfate particle population. In a second set of experiments (labeled “II”; Table 1), the surface area concentration of the ammonium sulfate particle population was stepwise decreased in the CMFR inflow, and after the chamber came to steady state the outflow S also decreased. Table 1 lists the relevant parameters and observations for both sets of experiments. The experiments carried out in the absence of ammonium sulfate particles (i.e., Exp. I-1 and II-7) corresponded to the lowest outflow S . New particle production occurred inside the CMFR for this case. The organic mass concentrations M_{org} and the yields Y_{org} listed in Table 1 represent adjustments of +37% to the AMS observations for correction of the deposition of particles to the bag walls. This

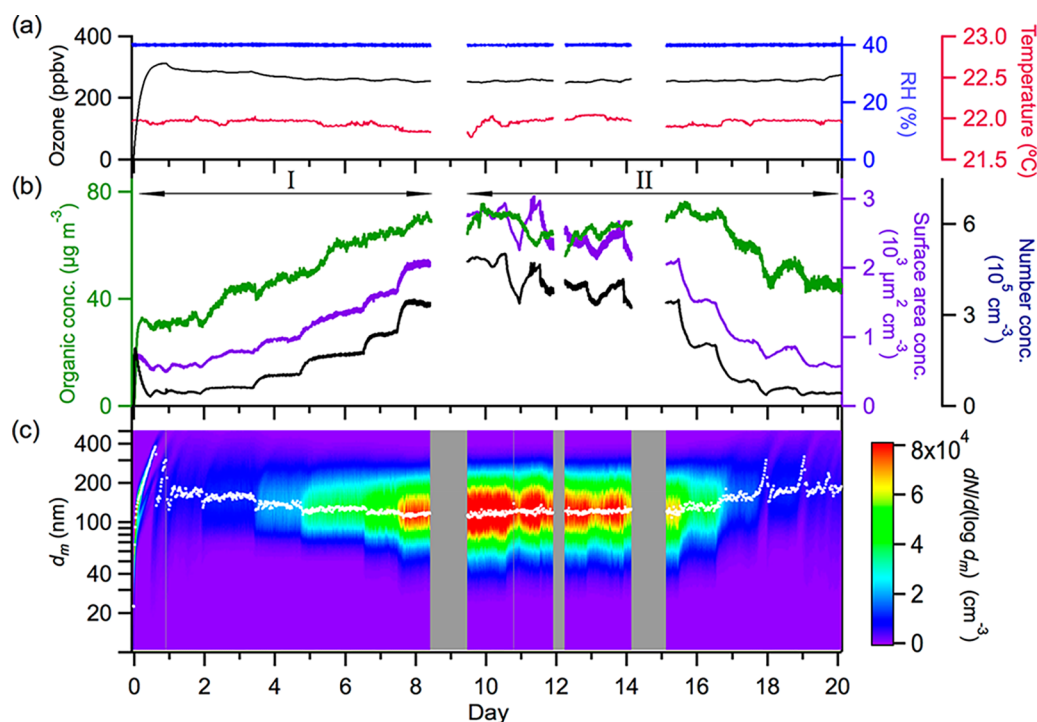


Figure 1. Time series of (a) ozone concentration, relative humidity, and temperature, (b) organic particle mass concentration measured by an Aerodyne high-resolution time-of-flight aerosol mass spectrometer (HR-ToF-AMS), particle surface area concentration and particle number concentration measured by a scanning mobility particle sizer (SMPS), and (c) particle number-diameter distributions measured by the SMPS. Further information on instrument operation is presented in the SI (Section S1). In panel c, the mode diameter of the distribution is plotted as white dots. Gray regions indicate absence of data because of technical problems. The presented time series include all experiments listed in Table 1. The time periods of experiment sets I and II are marked in panel b.

wall-loss correction factor was obtained from the loss rate of dried monodisperse ammonium sulfate particles injected in the chamber bag at 40% RH.⁵

Figure 1 presents the time series of results from both sets of experiments. Temperature, RH, and ozone concentration varied negligibly during the experiments (Figure 1a). Outflow S increased stepwise from (0.55 ± 0.03) to $(2.06 \pm 0.05) \times 10^3 \mu\text{m}^2 \text{cm}^{-3}$ during set I and then decreased from (2.87 ± 0.04) to $(0.58 \pm 0.01) \times 10^3 \mu\text{m}^2 \text{cm}^{-3}$ during set II (Figure 1b). Outflow M_{org} varied from 30.5 ± 0.6 to $71.5 \pm 0.7 \mu\text{g m}^{-3}$ during these experiments, corresponding to apparent PM yields of $(24.5 \pm 0.7)\%$ to $(57.4 \pm 0.8)\%$. Here, apparent yield is the ratio of the produced M_{org} to the reacted α -pinene mass concentration.⁸ Outflow particle number concentrations ranged from (4.2 ± 0.1) to $(49.2 \pm 0.9) \times 10^3 \text{cm}^{-3}$. The diameter-number distributions are plotted in Figure 1c. The particle mode diameters were 180 and 120 nm for experiments at lowest and highest S , respectively. Particles smaller than 30 nm were rare across the studied S , indicating that condensational growth dominated over new particle formation both in the presence and absence of the ammonium sulfate particles.

PM yield as a function of particle S is plotted in Figure 2 for experiment sets I and II. The apparent yield increased from 25% to 57% across the studied range of S . It became independent of S (i.e., the curve became flat) at a threshold concentration S^* of $2.1 \times 10^3 \mu\text{m}^2 \text{cm}^{-3}$, corresponding to a surface area ratio of 6×10^{-4} between the suspended particles and the Teflon bag of the reactor. For comparison, this S^* value is higher than commonly observed at various urban^{22–24} and rural/remote^{25–27} locations worldwide (Figure 2), although wall effects are mostly absent in the atmospheric context except near the planetary surface.

Experiment sets I and II also demonstrate a hysteresis with respect to the direction of changes in S . For the same S , yields were lower for set I conducted in the direction of stepwise increases in S compared to set II conducted in the direction of stepwise decreases in S (Table 1). Differences in apparent yield between sets I and II reached up to -11% (absolute difference) for the lowest S . This difference should be insignificantly affected by the difference in the pre-existing organic mass concentration of individual experiments, given that the initial pre-existing particles have been mostly replaced by the produced PM after one residence time. Apparent yields were the same within observational limits for $S > S^*$.

3.2. Gas-Particle, Gas-Wall, and Particle-Wall Cross Interactions. 3.2.1. Characteristic Timescales of Interactions.

The analysis herein considers the timescale τ_{gp} for gas-particle equilibrium partitioning and the timescale τ_{gw} for gas-wall deposition, the total time τ_{exp} for the complete set of experiments, the mean residence time τ_{res} of particles in the CMFR, and the characteristic time τ_{rxn} of chemical reactions for producing condensable vapors. The latter three had values as follows. The complete set of experiments took place across 20 days, that is, $\tau_{\text{exp}} = 2.9 \times 10^4$ min. The residence times of individual particles were described by Poisson statistics in the CMFR,¹⁹ with a mean value of $\tau_{\text{res}} = 270$ min. Condensable vapors from α -pinene ozonolysis were produced under pseudo-first-order conditions, corresponding to $\tau_{\text{rxn}} = (k [\text{O}_3])^{-1} = 26$ min for a bimolecular rate constant k of $8.66 \times 10^{-17} \text{cm}^3 \text{molecule}^{-1} \text{s}^{-1}$ between α -pinene and 300 ppb ozone.²⁸ For α -pinene ozonolysis, most condensable products by mass were first-generation products,²⁹ and they were thus produced within the time period τ_{rxn} or a short multiple of it. Additional reactions

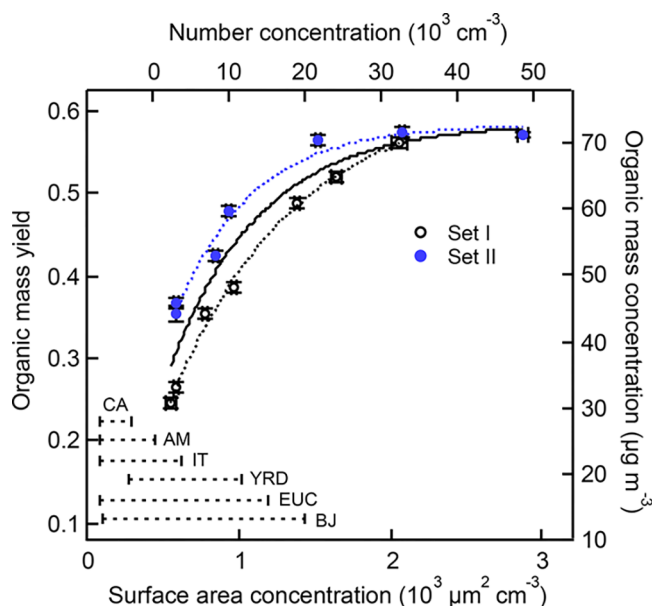


Figure 2. Apparent yield (left axis) and mass concentration (right axis) of PM as a function of particle surface area concentration S . Data points and uncertainty bars represent the mean values and one standard deviation, respectively, of the measurements across the last 6 h of each experiment. Experiment sets I and II (cf. Table 1) correspond to increasing and decreasing S in the CMFR, respectively. The thick solid line represents an empirical fit through all data points. The black and blue dotted lines represent the empirical fits of data points from experiment sets I and II, respectively. Particle number concentrations during the experiments are presented on the top axis. For comparison, S observed at various locations worldwide are also plotted (BJ: Beijing,²² EUC: European continent,²⁵ YRD: Yangtze River Delta,²³ IT: Italy,²⁴ AM: Amazon,²⁶ and CA: Sierra Nevada Mountains of California²⁷).

by hydroxyl radicals produced from side reactions or particle-phase reactions took place on a slower timescale,³⁰ and the analysis herein assumes that those reactions did not contribute significant additional condensable mass concentration. Thus, the chemical reactions to produce condensable vapors went to completion in the outflow of the CMFR as $\tau_{\text{rxn}} \ll \tau_{\text{res}}$.

In respect to gas-particle interactions, the time τ_{gp} for each gas-phase molecule to have one mass accommodation with a particle surface was estimated as follows:²⁸

$$\tau_{\text{gp}} = \frac{1}{2\pi N d_p D_g F_{\text{FS}}} \quad (1)$$

where N is the particle number concentration, d_p is particle diameter, D_g is the gas phase diffusivity, and F_{FS} is the Fuchs-Sutugin correction factor for noncontinuum gas-phase diffusion. F_{FS} depends on the gas-particle mass accommodation coefficient α_{gp} . Here, α_{gp} reflects the overall resistances of vapor molecules transferring into the particle bulk, including possible limits both by surface accommodation and particle-phase diffusion. Further equations are presented in SI Section 2. The functional form of τ_{gp} results as $\tau_{\text{gp}}(S(N, d_p), \alpha_{\text{gp}})$. As a caveat, although an aerosol (consisting of many gas-phase products with different values of α_{gp} and particles with many diameters d_p) is described in detail by a spectrum of τ_{gp} values, the analysis herein assumes that the aerosol can be adequately described in reference to factors affecting particle mass concentration by an average condensing product characterized by a single α_{gp} and an average particle

diameter characterized by single d_p , resulting in a single effective value of τ_{gp} .

In respect to gas-wall interactions, the time τ_{gw} for each gas-phase molecule to have one mass accommodation with the wall was estimated as follows:³¹

$$\tau_{\text{gw}} = \left(\frac{A}{V} \frac{\alpha_{\text{gw}} \bar{c} / 4}{1 + \pi \alpha_{\text{gw}} \bar{c} / 8 \sqrt{D_g K}} \right)^{-1} \quad (2)$$

where A is the surface area of the bag, V is its volume, \bar{c} is the mean thermal speed of the gas-phase molecules, and K is eddy diffusivity of the fluid in the bag. A K value of 0.22 s^{-1} was estimated for the studied CMFR based on the rates of particle deposition to the walls.¹⁴ The gas-wall mass accommodation coefficient α_{gw} was estimated by³²

$$\log_{10} \alpha_{\text{gw}} = -0.1919 \log_{10} C_i^* - 6.32 \quad (3)$$

Although the multiple gas-phase products with different values of C_i^* and α_{gw} values corresponds in detail to a spectrum of τ_{gw} values, the analysis herein assumes that an average condensing product characterized by a single α_{gw} is an adequate description, resulting in a single effective value of τ_{gw} . The saturation concentration C_i^* of the single effective product was estimated by considering the spectrum of C_i^* for the many condensable products i . The gas-phase chemistry of α -pinene ozonolysis was simulated using the Master Chemical Mechanism (MCM, version 3.3),³³ from which the oxidation products were obtained. The vapor pressures of those products were then estimated using a simple group contribution method (SIMPOL).³⁴ The major condensable products in the simulation correspond to C_i^* values across the range of $(0.8 \text{ to } 3.5) \times 10^3 \mu\text{g m}^{-3}$ and with a weighted mean of $660 \mu\text{g m}^{-3}$. For this mean C_i^* , the α_{gw} value was calculated as 2.8×10^{-6} and a τ_{gw} value of 42 min was obtained. Furthermore, during the experimental period of 20 days, the α_{gw} value remained distinct from the α_{gp} value because the walls remained sparsely laden with organic material (i.e., a thickness of approximately 0.48 nm; see SI Section S3), as justified by absorption of organic mass into the Teflon material of the walls.¹² During the experimental campaign across time τ_{exp} , the τ_{gw} was assumed to be a fixed quantity whereas τ_{gp} was varied by stepwise increases and decreases in S .

The functional form of $\tau_{\text{gp}}(S(N, d_p), \alpha_{\text{gp}})$ in relation to S and α_{gp} is conceptualized within the τ_{res} of the CMFR, as plotted in Figure 3. The gas-particle partitioning can be divided into two primary regimes by comparing the timescale τ_{gp} with the timescales τ_{rxn} and τ_{gw} . For $\tau_{\text{gp}} > \tau_{\text{gw}}$, defined as Regime 1, a high dependence of organic PM yield on S was expected because gas-particle partitioning was largely competitive with gas-wall interactions and substantial organic mass can be scavenged to the bag walls. This condition holds for large $\tau_{\text{gp}}(S(N, d_p), \alpha_{\text{gp}})$, meaning small N , d_p , or α_{gp} according to eq 1. The measured organic PM mass was thus sensitive to S in Regime 1. As τ_{gp} decreases for increasing S , the gas-wall interactions were reduced gradually and less organic mass was scavenged to the walls. For $\tau_{\text{gp}} < \tau_{\text{rxn}}$, defined as Regime 2, in the absence of any other process taking precedence, τ_{gp} was the ultimate limit for gas-particle partitioning equilibrium and organic mass was rarely scavenged to the walls. The PM yield was thus insensitive to S and the gas-particle partitioning was governed solely by the total produced condensable organic mass. Therefore, quasi-equilibrium growth¹⁶ occurred for the production of organic PM in Regime 2. The region between Regimes 1 and 2, that is, for $\tau_{\text{gp}} >$

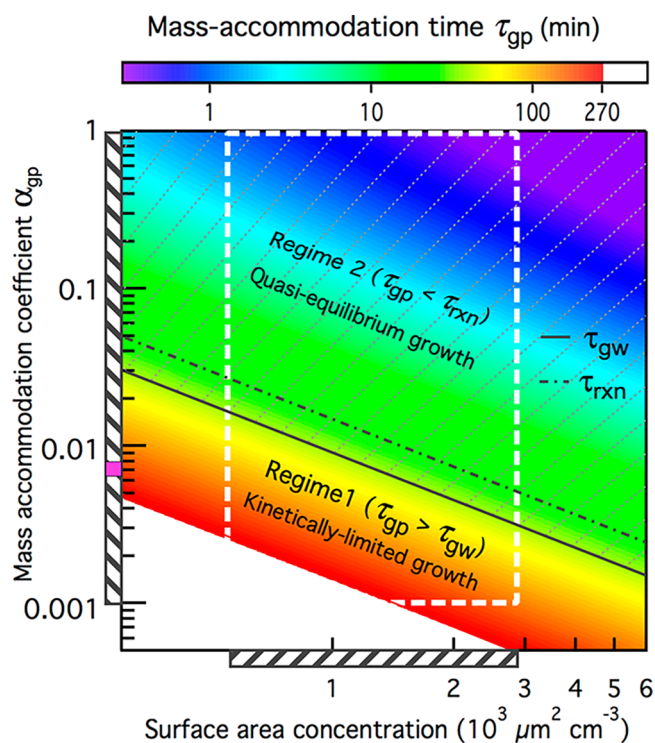


Figure 3. Comparative timescales of gas-particle interactions and gas-wall interactions. The gas-particle mass accommodation time $\tau_{gp}(S(N, d_p), \alpha_{gp})$ of eq 1 is represented in false color as a bivariate function of particle surface area concentration S and gas-particle mass accommodation coefficient α_{gp} . The coloring corresponds to d_p of 120 nm and D_g of $3 \times 10^{-6} \text{ m}^2 \text{ s}^{-1}$. The solid and dashed lines represent the estimates of τ_{gw} (42 min) and τ_{rxn} (26 min), respectively. In regime 1, gas-particle mass accommodation is slower than gas-wall mass accommodation (i.e., $\tau_{gp} > \tau_{gw}$). In regime 2, chemical reactions for producing condensable vapors is slower than gas-particle mass accommodation (i.e., $\tau_{gp} < \tau_{rxn}$), and the apparent PM yield is independent of S in this regime. The heavy hatching represents the regime with less gas-wall deposition effect (i.e., $\tau_{gp} < \tau_{gw}$). The shading on the abscissa represents the range of S for experiment sets I and II. The shading on the ordinate represents the range of α_{gp} reported in the literature for α -pinene ozonolysis.^{13,16,36,37} The solid magenta square marker on the ordinate represents the best estimate of α_{gp} for the data sets of this study. The white dashed box represents the overlap region of the abscissa and ordinate shadings. For the white blank region, the time for gas-particle mass accommodation is slower than the CMFR residence time (i.e., $\tau_{gp} > \tau_{res}$ of 270 min).

τ_{rxn} but $\tau_{gp} < \tau_{gw}$, was a transition from kinetically limited Regime 1 to quasi-equilibrium Regime 2 with the increase of S . Here, the gas-particle partitioning remains governed by the timescale τ_{gp} while the gas-wall interactions were much less, for which the PM yield depended only weakly on S compared to those in Regime 1.

The critical value S^* for the independence of apparent PM yield on S represents the yield in the absence of significant mass scavenging to the walls. The dashed white box in Figure 3 represents the S studied in the current work with an gas-particle mass accommodation coefficient α_{gp} from 0.001 to 1, as reported previously for α -pinene ozonolysis.^{13,15,35–38} According to the critical value S^* of $2.1 \times 10^3 \mu\text{m}^2 \text{ cm}^{-3}$ in the data sets of Figure 2, an optimal α_{gp} value of 0.007 (i.e., the magenta marker in Figure 3) is required to eliminate the kinetic limitation of both gas-particle and gas-wall interactions. Note that this estimation did not account for the evaporation of gas phase material from the particles and walls. This value is close to the accommodation

coefficient of 0.001–0.01 derived by measuring the evaporation rate of organic PM from α -pinene ozonolysis using isothermal dilution,³⁵ while lower than those of order 0.1 derived from several studies using thermal denuders^{37,39} and a batch-mode reactor.¹⁵ It is also in the range of 0.002–0.05 required to simulate the evaporation of organic PM from the ozonolysis of several monoterpenes (including α -pinene).³⁶ This value is much lower than an α_{gp} of unity reported for α -pinene ozonolysis in a continuously stirred flow reactor,¹³ in which organic PM was dominated primarily by extremely low-volatility organic compounds. This value is also on the same order as those of 0.001 for organic PM from toluene photooxidation,¹⁴ despite the mechanisms for organic PM production are totally different for toluene and α -pinene. Nevertheless, to discern the reasons for the different α_{gp} is more complicated, given that the experimental configurations and the approaches of deriving this value are different for individual studies.

3.2.2. Irreversible and Reversible Processes. The characteristic timescales discussed above assumes irreversible gas-particle and gas-wall interactions without accounting for gas-phase evaporation from the surfaces of the particles and the walls. The actual processes occurred in the CMFR might have been slightly different. The following definitions are proposed for further illustration. The total condensable organic mass concentration M_{org}^{total} produced from α -pinene ozonolysis spreads between organic mass concentration M_{org}^f in outflow of the CMFR and organic mass on the bag walls that remain in the CMFR. More specifically, M_{org}^f represents the quantity measured by the AMS including positive correction for particle deposition of the walls and is same as M_{org} elsewhere in this study. The quantity $(1 - M_{org}^f/M_{org}^{total})$ represents the fraction of the PM mass yield that remains on the walls, thereby reducing the apparent yield in the reactor outflow. The ratio of $M_{org}^f/M_{org}^{total}$ thus represents a yield correction factor for apparent yield and this factor goes to unity in the absence of gas-wall loss. The conditional scope considered herein is that both τ_{gp} and τ_{gw} are less than τ_{res} and most of the produced condensable species are deposited on a combination of the walls and the particle surfaces just after the shorter of τ_{gp} or τ_{gw} . During the experimental campaign, τ_{gw} was assumed to be a fixed quantity whereas τ_{gp} was varied by stepwise increases and decreases in S .

For irreversible interaction case, $M_{org}^f/M_{org}^{total}$ increased stepwise with the increase of S for $S < S^*$ (i.e., $\tau_{gp} > \tau_{gw}$ in the Regime 1 of Figure 3). The $M_{org}^f/M_{org}^{total}$ approached unity for $S > S^*$ (i.e., $\tau_{gp} < \tau_{rxn}$ in the Regime 2). In respect to the history of increasing or decreasing S in experiments, there should be no difference in $M_{org}^f/M_{org}^{total}$ for a fully irreversible interaction. However, the apparent PM yield of experiment sets I and II shows hysteresis (Figure 2). Given that experiment set II was conducted after set I, the differences in apparent PM yield might have been resulted from the gas-particle, gas-wall, and particle-wall cross interactions involving some reversible processes¹² inside the CMFR.

For reversible gas-particle and gas-wall interactions (i.e., facile absorption and desorption), the initial deposition at the timescale τ_{rxn} was unchanged compared to those of irreversible case. Beyond this initial period up to τ_{res} , the gas phase continuously reversibly exchanges in a complex manner both with the particle material and the material deposited to the bag walls. We use M_{org}^{equi} here to represent the organic mass concentration of full equilibrium composition established between the particle material and the material on the walls. After the timescale τ_{rxn} of initial deposition, the M_{org}^f evolved

toward $M_{\text{org}}^{\text{equi}}$ based on multistep deposition and evaporation. For $\tau_{\text{gp}} > \tau_{\text{gw}}$ (i.e., low S), the yield correction factor $M_{\text{org}}^{\text{f}}/M_{\text{org}}^{\text{total}}$ depended strongly on S and moderately on $M_{\text{org}}^{\text{equi}}$. The $M_{\text{org}}^{\text{equi}}$ was possibly varied with the experimental history, specifically from the amount and type of material deposited to and evaporated from the walls. The hysteresis in the apparent yield thus can be explained by the different $M_{\text{org}}^{\text{equi}}$ values due to the larger influence of the organic material released from the bag walls in experiment set II. For $\tau_{\text{gp}} < \tau_{\text{rxn}}$ (i.e., sufficiently high S), the $M_{\text{org}}^{\text{f}}/M_{\text{org}}^{\text{total}}$ was governed primarily by the total produced condensable organic mass and thus the influence of the material on the bag walls to $M_{\text{org}}^{\text{equi}}$ was relatively small. Given that the products from α -pinene ozonolysis were across a wide spectrum of volatilities, actual processes occurred in the CMFR were most likely a mix of irreversible and reversible interactions. The expectation is that the deposited material on the bag walls mostly served as a reservoir that grew continually in experiment set I and evaporated at least partially in set II.

3.3. Effect of Surface Area Concentration on Chemical Composition. The PM chemical composition for variable particle S was investigated based on the mass spectra. The fractional distribution of the C_xH_y^+ , $\text{C}_x\text{H}_y\text{O}_1^+$, and $\text{C}_x\text{H}_y\text{O}_2^+$ families are plotted in Figure 4a. The $\text{C}_x\text{H}_y\text{O}_2^+$ family decreased from 24% to 17% of the total organic signal from low to high S for $S < S^*$ and remained constant at 17% for higher S . The contribution of the C_xH_y^+ family correspondingly increased from 45% to 51%. The contribution of the $\text{C}_x\text{H}_y\text{O}_1^+$ appeared unchanged between 31% and 33% with S . Related trends in the

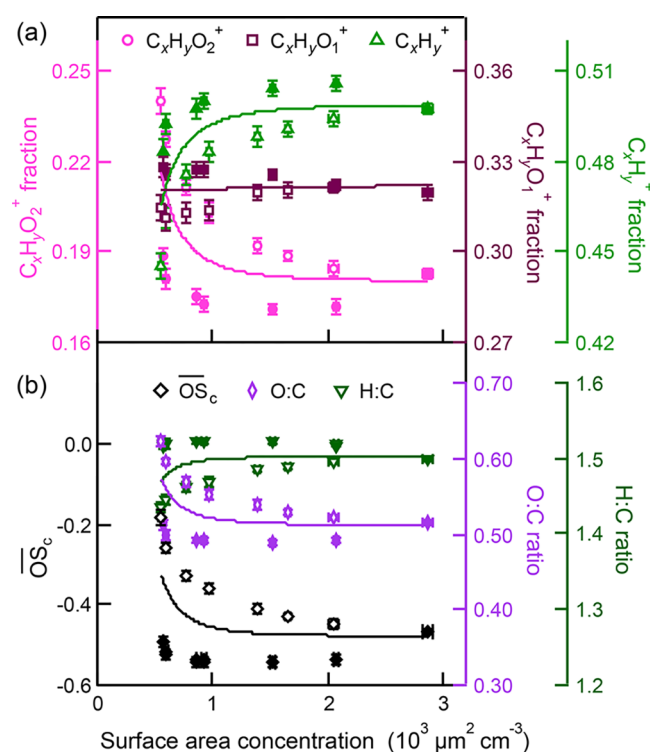


Figure 4. (a) Fractional contribution of $\text{C}_x\text{H}_y\text{O}_2^+$, $\text{C}_x\text{H}_y\text{O}_1^+$, and C_xH_y^+ families as a function of S . (b) Carbon oxidation state $\overline{\text{OS}}_c$, O:C elemental ratio, and H:C elemental ratio. Experiment sets I and II (cf. Table 1) are denoted by open and closed symbols, respectively. Data points and uncertainty bars represent the mean values and one standard deviation, respectively, of the measurements across the last 6 h of each experiment. Data are available in SI Table S1.

oxygen-to-carbon (O:C) atomic ratio, the hydrogen-to-carbon (H:C) atomic ratio, and the carbon oxidation state ($\overline{\text{OS}}_c$, calculated by $2 \times \text{O:C} - \text{H:C}$)⁴⁰ are plotted in Figure 4b. For set I, from low to high S for $S < S^*$, the $\overline{\text{OS}}_c$ and the O:C ratio decreased whereas the H:C ratio increased. For set II, these quantities changed negligibly in S within experimental uncertainty. The results for set I suggest that less-oxidized, more-volatile organic species have a greater sensitivity to gas-particle-wall cross interactions for $S < S^*$ than do those of more-oxidized, less-volatile organic species. The hysteresis difference between set I and set II also supports this interpretation because the more-volatile species are closer to saturation with the material on the walls in the later experiments. They are thus scavenged to a lesser extent to the walls. The further implication is to support an interpretation of a reversible process, at least in part, in the particle-wall cross interactions.

3.4. Comparison with Other Studies. A comparison of the mass concentration and yield of PM influenced by S from this study with those reported in literature is summarized in Table 2.^{12–16,32,38,41–45} A common feature across most of these studies, which differed in bag sizes and operation modes, is that the PM mass concentration and yield were affected by the link between gas-wall and gas-particle interactions. In some cases, yield was affected by up to 400% depending on experimental conditions and reaction properties.^{14,42} The dependence of yield on S in these studies could mostly be explained by the loss of condensable organic vapors to the bag walls. Yield independent of S was also reported for PM production dominated by quasi-equilibrium growth.¹⁵

Changes in chemical composition for increasing particle S also have been reported previously (Table 2).^{12,32,41,43–45} For the batch-mode experiments, the highest gas-wall loss rates were observed for highly oxidized, low-volatility compounds.^{12,32,41,43} More-oxidized PM was obtained because of greater relative deposition of those gas-phase products onto particle surfaces rather than to the bag walls for increasing S . This behavior is opposite to the observations of current study using the CMFR, for which less-oxidized PM was enhanced for increasing S in set I. A possible explanation is that a higher S not only limits the gas-wall interactions of more-oxidized organic species but also largely facilitate the gas-particle partitioning of less-oxidized species, and the latter effect might greatly overwhelm the former in the CMFR compared to those of batch-mode reactors. The gas-phase chemistry of PM production for individual VOCs could also differ between the batch-mode and the CMFR reactors.

The influence of S on the production and the composition of organic PM in general differs to a certain extent among previous studies, which can possibly be explained by the discrepancies in both the characteristics of the reactors and the experimental conditions. Contrary to the continuous oxidation of products over a certain time period in batch-mode reactors, the role of less-oxidized species from multiple gas-phase chemical routes might be more important in CMFRs, as observed in the current work. Reactor dimensions also possibly influence the gas-wall interactions, which is indicated by the ratio of surface area to volume of the chamber bag (A/V) in eq 2 above. Experimental conditions such as temperature, RH, and the reactant and oxidant composition could also influence the properties of organic PM, such as their physical state, oxidation state, and production rate, and these factors can lead to differences in dependence on particle surface area among the individual

Table 2. Comparison across Literature of the Mass Concentrations, Yields, and Other Characteristics of Particle Populations as Influenced by Surface Area Concentration and Gas-Wall Loss

| mode of operation | bag volume (m ³) | precursor VOC | temp. (°C) | RH (%) | pre-existing particle population | surface area concentration (10 ³ μm ² cm ⁻³) | effects on organic PM mass concentration and apparent yield | effects on other characteristics | reference |
|-------------------|------------------------------|--|------------|--------|---|--|---|---|------------|
| batch | 28 | 2,3-epoxy-1,4-butanediol and glyoxal; no reactions | 20 | dry<61 | (NH ₄) ₂ SO ₄ +H ₂ SO ₄ | na | | gas-wall loss rate may depend on the molecular structure of the compound | 41 |
| batch | 5.9, 1.7 | alkanes, alkenes, alcohols, and ketones; no reactions | 25 | <1 | none | na | 0–65% of organic carbon partitioned to the bag walls at equilibrium | gas-wall loss increased with increasing carbon number within an organic class. It increased in the order of <i>n</i> -alkanes <1-alkenes <2-alcohols <2-ketones for organics having similar vapor pressures | 12 |
| batch | 4 | α -pinene; ozonolysis | 25 | 5 | (NH ₄) ₂ SO ₄ | 0.416 | yield can be underestimated by up to a factor of 4 due to wall loss of oxidized VOCs | | 42 |
| batch | 24 | toluene; photooxidation; high- and low-NO _x | 25 | 3% | (NH ₄) ₂ SO ₄ | 0–10 | yield can be underestimated by factors as high as 4 | | 14 |
| batch | 24 | α -pinene; isoprene, dodecane, and toluene; photooxidation; high- and low-NO _x | 25–45 | dry | none | na | the effect on yield depended on the competition between gas-particle and gas-wall interactions | highly oxygenated and least volatile compounds had the maximum wall-loss rate | 32 |
| batch | 24 | α -pinene; ozonolysis | na | na | (NH ₄) ₂ SO ₄ , NaNO ₃ | 1–5 | | the carbon oxidation state of PM increased with increasing the surface area of pre-existing particle population | 43 |
| batch | 13 | α -pinene; ozonolysis | 25 | <5 | (NH ₄) ₂ SO ₄ | 0–2.72 | yield was independent of particle surface area concentration. | | 15 |
| batch | 24 | α -pinene; photooxidation; low-NO | 25 | <5 | (NH ₄) ₂ SO ₄ | 0–3.4 | the growth curves of organic PM as a function of reacted α -pinene essentially overlapped for different initial seed particle concentration | | 38 |
| batch | 10 | alkanes, oleic acid, and levoglucosan; no reactions | 22–44 | na | (NH ₄) ₂ SO ₄ | na | | the gas-wall loss rates of SVOCs were significant, quasi-irreversible, and proportional to the SVOC concentrations | 45 |
| box model | | toluene; photooxidation | 25 | | inorganics | 0.44–26 | gas-wall deposition decreased particle yield | surface area dependence is present when condensation is kinetically limited | 16 |
| box model | | alkanes or alkenes; photooxidation; high-NO _x | | | diethylsebacate | | yield could be underestimated by up to a factor of 2 | nitrate, hydroxynitrate, and carbonyl esters could be substantially lost onto bag walls | 44 |
| CMFR | 1.45 | α -pinene; ozonolysis | 16 | 63 | (NH ₄) ₂ SO ₄ | 0.02–1 | particle organic mass concentration contributed by extremely low-volatility organic compounds increased with increasing particle surface area concentration | | 13 |
| CMFR | 4.7 | α -pinene; ozonolysis | 22 | 40 | (NH ₄) ₂ SO ₄ | 0.55–2.87 | yield increased by up to 2.3 times with increasing particle surface area concentration | mass concentration of less-oxygenated PM increased with increasing particle surface area concentration | this study |

studies. Future studies related to the two types of reactors operated under similar conditions will be important for explaining the apparent differences, and these comparative insights could be helpful in further understanding the particle-wall cross connections in PM production.

3.5. Atmospheric Implications. The condensational growth of organic particulate matter in the CMFR was influenced by the competition of gas-particle, gas-wall, and particle-wall cross interactions. An increasing surface area concentration S led to increased PM production, mostly because of greater partitioning of semivolatile organic species to the particle phase. Laboratory studies concerned with PM yield are advised to carry out control experiments to establish that the reported yields correspond to $S > S^*$, which can be considered as the prevailing atmospheric condition except possibly for near the planetary surface.

The experiments in the current work focused on the influence of S on the apparent PM yield of α -pinene ozonolysis. The influence of S on PM produced from other hydrocarbon precursors deserves further investigation because of the tight coupling of τ_{gp} , τ_{gw} , and τ_{res} with respect to reaction chemistry and chamber operation modes. The analysis herein assumed that in-particle slow processes such as diffusivity, as related to particle viscosity, were faster than τ_{gp} , τ_{gw} , and τ_{res} . A relevant topic worth additional investigation is how semisolid and solid PM can influence apparent yields, especially at low RH that many chamber experiments have historically been conducted.⁴⁶ A further topic that remains technically challenging is the assessment of gas-wall interactions for the myriad of atmospheric organic compounds given that the analysis herein assumed a single effective species. Finally, temperature and RH were fixed in the experiments herein, whereas both can be important variables influencing τ_{gp} and τ_{gw} as well as properties of organic PM. Further experiments testing how the uninvestigated factors of the present study influence apparent yield while varying S are warranted for quantitatively characterizing the role of gas-particle, gas-wall, and particle-wall cross interactions.

■ ASSOCIATED CONTENT

Supporting Information

The Supporting Information is available free of charge on the ACS Publications website at DOI: 10.1021/acs.est.8b07302.

Relevant information on experimental methods, additional equations of gas-particle interactions, estimation of organic material on the Teflon bag walls, Table S1, and Figure S1 (PDF)

■ AUTHOR INFORMATION

Corresponding Authors

*(Y.H.) E-mail: yuemei.han@ieecas.cn.

*(S.T.M.) E-mail: scot_martin@harvard.edu.

ORCID

Yuemei Han: 0000-0002-5044-8386

Zhaoheng Gong: 0000-0002-9451-2060

Pengfei Liu: 0000-0001-7280-9720

Present Address

‡(K.A.M.) Department of Chemistry, Colby College, Waterville, Maine 04901, United States.

Notes

The authors declare no competing financial interest.

■ ACKNOWLEDGMENTS

This study was funded by the Division of Atmospheric and Geospace Sciences of the U.S. National Science Foundation (Grant 1640378) and the Office of Science of the U.S. Department of Energy (Grant DE-SC0012792).

■ REFERENCES

- (1) Abbatt, J.; George, C.; Melamed, M.; Monks, P.; Pandis, S.; Rudich, Y. New Directions: Fundamentals of Atmospheric Chemistry: Keeping a Three-Legged Stool Balanced. *Atmos. Environ.* **2014**, *48*, 390–391.
- (2) Burkholder, J. B.; Abbatt, J. P. D.; Barnes, I.; Roberts, J. M.; Melamed, M. L.; Ammann, M.; Bertram, A. K.; Cappa, C. D.; Carlton, A. G.; Carpenter, L. J.; Crowley, J. N.; Dubowski, Y.; George, C.; Heard, D. E.; Herrmann, H.; Keutsch, F. N.; Kroll, J. H.; McNeill, V. F.; Ng, N. L.; Nizkorodov, S. A.; Orlando, J. J.; Percival, C. J.; Picquet-Varrault, B.; Rudich, Y.; Seakins, P. W.; Surratt, J. D.; Tanimoto, H.; Thornton, J. A.; Tong, Z.; Tyndall, G. S.; Wahner, A.; Weschler, C. J.; Wilson, K. R.; Ziemann, P. J. The Essential Role for Laboratory Studies in Atmospheric Chemistry. *Environ. Sci. Technol.* **2017**, *51*, 2519–2528.
- (3) Cocker, D. R.; Flagan, R. C.; Seinfeld, J. H. State-of-the-Art Chamber Facility for Studying Atmospheric Aerosol Chemistry. *Environ. Sci. Technol.* **2001**, *35*, 2594–2601.
- (4) Carter, W. P. L.; Cocker, D. R.; Fitz, D. R.; Malkina, I. L.; Bumiller, K.; Sauer, C. G.; Pisano, J. T.; Bufalino, C.; Song, C. A New Environmental Chamber for Evaluation of Gas-Phase Chemical Mechanisms and Secondary Aerosol Formation. *Atmos. Environ.* **2005**, *39*, 7768–7788.
- (5) Shilling, J. E.; Chen, Q.; King, S. M.; Rosenoern, T.; Kroll, J. H.; Worsnop, D. R.; McKinney, K. A.; Martin, S. T. Particle Mass Yield in Secondary Organic Aerosol Formed by the Dark Ozonolysis of α -Pinene. *Atmos. Chem. Phys.* **2008**, *8*, 2073–2088.
- (6) Shilling, J. E.; Chen, Q.; King, S. M.; Rosenoern, T.; Kroll, J. H.; Worsnop, D. R.; DeCarlo, P. F.; Aiken, A. C.; Sueper, D.; Jimenez, J. L.; Martin, S. T. Loading-Dependent Elemental Composition of α -Pinene SOA Particles. *Atmos. Chem. Phys.* **2009**, *9*, 771–782.
- (7) Leskinen, A.; Yli-Pirilä, P.; Kuusalo, K.; Sippula, O.; Jalava, P.; Hirvonen, M.-R.; Jokiniemi, J.; Virtanen, A.; Komppula, M.; Lehtinen, K. E. J. Characterization and Testing of a New Environmental Chamber. *Atmos. Meas. Tech.* **2015**, *8*, 2267–2278.
- (8) Odum, J. R.; Hoffmann, T.; Bowman, F.; Collins, D.; Flagan, R. C.; Seinfeld, J. H. Gas Particle Partitioning and Secondary Organic Aerosol Yields. *Environ. Sci. Technol.* **1996**, *30*, 2580–2585.
- (9) Chan, M. N.; Chan, A. W. H.; Chhabra, P. S.; Surratt, J. D.; Seinfeld, J. H. Modeling of Secondary Organic Aerosol Yields from Laboratory Chamber Data. *Atmos. Chem. Phys.* **2009**, *9*, 5669–5680.
- (10) Pye, H. O. T.; Chan, A. W. H.; Barkley, M. P.; Seinfeld, J. H. Global Modeling of Organic Aerosol: The Importance of Reactive Nitrogen (NO_x and NO₃). *Atmos. Chem. Phys.* **2010**, *10*, 11261–11276.
- (11) Valorso, R.; Aumont, B.; Camredon, M.; Raventos-Duran, T.; Mouchel-Vallon, C.; Ng, N. L.; Seinfeld, J. H.; Lee-Taylor, J.; Madronich, S. Explicit Modelling of SOA Formation from α -Pinene Photooxidation: Sensitivity to Vapour Pressure Estimation. *Atmos. Chem. Phys.* **2011**, *11*, 6895–6910.
- (12) Matsunaga, A.; Ziemann, P. J. Gas-Wall Partitioning of Organic Compounds in a Teflon Film Chamber and Potential Effects on Reaction Product and Aerosol Yield Measurements. *Aerosol Sci. Technol.* **2010**, *44*, 881–892.
- (13) Ehn, M.; Thornton, J. A.; Kleist, E.; Sipilä, M.; Junninen, H.; Pullinen, I.; Springer, M.; Rubach, F.; Tillmann, R.; Lee, B.; Lopez-Hilfiker, F.; Andres, S.; Acir, I.-H.; Rissanen, M.; Jokinen, T.; Schobesberger, S.; Kangasluoma, J.; Kontkanen, J.; Nieminen, T.; Kurtén, T.; Nielsen, L. B.; Jørgensen, S.; Kjaergaard, H. G.; Canagaratna, M.; Maso, M. D.; Berndt, T.; Petäjä, T.; Wahner, A.; Kerminen, V.-M.; Kulmala, M.; Worsnop, D. R.; Wildt, J.; Mentel, T. F. A Large Source of Low-Volatility Secondary Organic Aerosol. *Nature* **2014**, *506*, 476–479.

- (14) Zhang, X.; Cappa, C. D.; Jathar, S. H.; McVay, R. C.; Ensberg, J. J.; Kleeman, M. J.; Seinfeld, J. H.; Christopher, D. Cappa. Influence of Vapor Wall Loss in Laboratory Chambers on Yields of Secondary Organic Aerosol. *Proc. Natl. Acad. Sci. U. S. A.* **2014**, *111*, 1–6.
- (15) Nah, T.; McVay, R. C.; Zhang, X.; Boyd, C. M.; Seinfeld, J. H.; Ng, N. L. Influence of Seed Aerosol Surface Area and Oxidation Rate on Vapor Wall Deposition and SOA Mass Yields: A Case Study with α -Pinene Ozonolysis. *Atmos. Chem. Phys.* **2016**, *16*, 9361–9379.
- (16) McVay, R. C.; Cappa, C. D.; Seinfeld, J. H. Vapor-Wall Deposition in Chambers: Theoretical Considerations. *Environ. Sci. Technol.* **2014**, *48*, 10251–10258.
- (17) Seinfeld, J. H.; Kleindienst, T. E.; Edney, E. O.; Cohen, J. B. Aerosol Growth in a Steady-State, Continuous Flow Chamber: Application to Studies of Secondary Aerosol Formation. *Aerosol Sci. Technol.* **2003**, *37*, 728–734.
- (18) Mentel, T. F.; Wildt, J.; Kiendler-Scharr, A.; Kleist, E.; Tillmann, R.; Dal Maso, M.; Fisseha, R.; Hohaus, T.; Spahn, H.; Uerlings, R.; Wegener, R.; Griffiths, P. T.; Dinar, E.; Rudich, Y.; Wahner, A. Photochemical Production of Aerosols from Real Plant Emissions. *Atmos. Chem. Phys.* **2009**, *9*, 4387–4406.
- (19) Martin, S. T.; Kuwata, M.; Smith, M. L. An Analytic Equation for the Volume Fraction of Condensationally Grown Mixed Particles and Applications to Secondary Organic Material Produced in Continuously Mixed Flow Reactors. *Aerosol Sci. Technol.* **2014**, *48*, 803–812.
- (20) Kang, E.; Root, M. J.; Toohey, D. W.; Brune, W. H. Introducing the Concept of Potential Aerosol Mass (PAM). *Atmos. Chem. Phys.* **2007**, *7*, 5727–5744.
- (21) Decarlo, P. F.; Kimmel, J. R.; Trimborn, A.; Northway, M. J.; Jayne, J. T.; Aiken, A. C.; Gonin, M.; Fuhrer, K.; Horvath, T.; Docherty, K. S.; Worsnop, D. R.; Jimenez, J. L. Field-Deployable, High-Resolution, Time-of-Flight Aerosol Mass Spectrometer. *Anal. Chem.* **2006**, *78*, 8281–8289.
- (22) Zhang, Y. M.; Zhang, X. Y.; Sun, J. Y.; Lin, W. L.; Gong, S. L.; Shen, X. J.; Yang, S. Characterization of New Particle and Secondary Aerosol Formation during Summertime in Beijing, China. *Tellus, Ser. B* **2011**, *63*, 382–394.
- (23) Gao, J.; Wang, T.; Zhou, X.; Wu, W.; Wang, W. Measurement of Aerosol Number Size Distributions in the Yangtze River Delta in China: Formation and Growth of Particles under Polluted Conditions. *Atmos. Environ.* **2009**, *43*, 829–836.
- (24) Buonanno, G.; Fuoco, F. C.; Stabile, L. Influential Parameters on Particle Exposure of Pedestrians in Urban Microenvironments. *Atmos. Environ.* **2011**, *45*, 1434–1443.
- (25) Müller, D.; Ansmann, A.; Wagner, F.; Franke, K.; Althausen, D. European Pollution Outbreaks during ACE 2: Microphysical Particle Properties and Single-Scattering Albedo Inferred from Multiwavelength Lidar Observations. *J. Geophys. Res.* **2002**, *107*, 1–11.
- (26) ARM Data Archive, <https://www.archive.arm.gov>.
- (27) Lunden, M. M.; Black, D. R.; McKay, M.; Revzan, K. L.; Goldstein, A. H.; Brown, N. J. Characteristics of Fine Particle Growth Events Observed above a Forested Ecosystem in the Sierra Nevada Mountains of California. *Aerosol Sci. Technol.* **2006**, *40*, 373–388.
- (28) Seinfeld, J. H.; Pandis, S. N. *Atmospheric Chemistry and Physics: From Air Pollution to Climate Change*, 2nd ed.; John Wiley Sons, Inc.: Hoboken, NJ, 2006.
- (29) Henry, K. M.; Lohaus, T.; Donahue, N. M. Organic Aerosol Yields from α -Pinene Oxidation: Bridging the Gap between First-Generation Yields and Aging Chemistry. *Environ. Sci. Technol.* **2012**, *46*, 12347–12354.
- (30) Kristensen, K.; Watne, Å. K.; Hammes, J.; Lutz, A.; Petäjä, T.; Hallquist, M.; Bilde, M.; Glasius, M. High-Molecular Weight Dimer Esters Are Major Products in Aerosols from α -Pinene Ozonolysis and the Boreal Forest. *Environ. Sci. Technol. Lett.* **2016**, *3*, 280–285.
- (31) McMurry, P. H.; Grosjean, D. Gas and Aerosol Wall Losses in Teflon Film Smog Chambers. *Environ. Sci. Technol.* **1985**, *19*, 1176–1182.
- (32) Zhang, X.; Schwantes, R. H.; McVay, R. C.; Lignell, H.; Coggon, M. M.; Flagan, R. C.; Seinfeld, J. H. Vapor Wall Deposition in Teflon Chambers. *Atmos. Chem. Phys.* **2015**, *15*, 4197–4214.
- (33) Saunders, S. M.; Jenkin, M. E.; Derwent, R. G.; Pilling, M. J. Protocol for the Development of the Master Chemical Mechanism, MCM v3 (Part A): Tropospheric Degradation of Non-Aromatic Volatile Organic Compounds. *Atmos. Chem. Phys.* **2003**, *3*, 161–180.
- (34) Pankow, J. F.; Asher, W. E. SIMPOL.1: A Simple Group Contribution Method for Predicting Vapor Pressures and Enthalpies of Vaporization of Multifunctional Organic Compounds. *Atmos. Chem. Phys.* **2008**, *8*, 2773–2796.
- (35) Grieshop, A. P.; Donahue, N. M.; Robinson, A. L. Is the Gas-Particle Partitioning in Alpha-Pinene Secondary Organic Aerosol Reversible? *Geophys. Res. Lett.* **2007**, *34*, L14810.
- (36) Lee, B.-H.; Pierce, J. R.; Engelhart, G. J.; Pandis, S. N. Volatility of Secondary Organic Aerosol from the Ozonolysis of Monoterpenes. *Atmos. Environ.* **2011**, *45*, 2443–2452.
- (37) Saleh, R.; Donahue, N. M.; Robinson, A. L. Time Scales for Gas-Particle Partitioning Equilibration of Secondary Organic Aerosol Formed from Alpha-Pinene Ozonolysis. *Environ. Sci. Technol.* **2013**, *47*, 5588–5594.
- (38) McVay, R. C.; Zhang, X.; Aumont, B.; Valorso, R.; Camredon, M.; La, Y. S.; Wennberg, P. O.; Seinfeld, J. H. SOA Formation from the Photooxidation of α -Pinene: Systematic Exploration of the Simulation of Chamber Data. *Atmos. Chem. Phys.* **2016**, *16*, 2785–2802.
- (39) Saha, P. K.; Grieshop, A. P. Exploring Divergent Volatility Properties from Yield and Thermodynamic Measurements of Secondary Organic Aerosol from α -Pinene Ozonolysis. *Environ. Sci. Technol.* **2016**, *50*, 5740–5749.
- (40) Kroll, J. H.; Donahue, N. M.; Jimenez, J. L.; Kessler, S. H.; Canagaratna, M. R.; Wilson, K. R.; Altieri, K. E.; Mazzoleni, L. R.; Wozniak, A. S.; Bluhm, H.; Mysak, E. R.; Smith, J. D.; Kolb, C. E.; Worsnop, D. R. Carbon Oxidation State as a Metric for Describing the Chemistry of Atmospheric Organic Aerosol. *Nat. Chem.* **2011**, *3*, 133–139.
- (41) Loza, C. L.; Chan, A. W. H.; Galloway, M. M.; Keutsch, F. N.; Flagan, R. C.; Seinfeld, J. H. Characterization of Vapor Wall Loss in Laboratory Chambers. *Environ. Sci. Technol.* **2010**, *44*, 5074–5078.
- (42) Kokkola, H.; Yli-Pirilä, P.; Vesterinen, M.; Korhonen, H.; Keskinen, H.; Romakkaniemi, S.; Hao, L.; Kortelainen, A.; Joutsensaari, J.; Worsnop, D. R.; Virtanen, A.; Lehtinen, K. E. J. The Role of Low Volatile Organics on Secondary Organic Aerosol Formation. *Atmos. Chem. Phys.* **2014**, *14*, 1689–1700.
- (43) Huang, D. D.; Zhang, X.; Dalleska, N. F.; Lignell, H.; Coggon, M. M.; Chan, C. M.; Flagan, R. C.; Seinfeld, J. H.; Chan, C. K. A Note on the Effects of Inorganic Seed Aerosol on the Oxidation State of Secondary Organic Aerosol- α -Pinene Ozonolysis. *J. Geophys. Res.* **2016**, *121*, 12,476–12,483.
- (44) La, Y. S.; Camredon, M.; Ziemann, P. J.; Valorso, R.; Matsunaga, A.; Lannuque, V.; Lee-Taylor, J.; Hodzic, A.; Madronich, S.; Aumont, B. Impact of Chamber Wall Loss of Gaseous Organic Compounds on Secondary Organic Aerosol Formation: Explicit Modeling of SOA Formation from Alkane and Alkene Oxidation. *Atmos. Chem. Phys.* **2016**, *16*, 1417–1431.
- (45) Ding, X.; Hofbauer, V.; Ye, P.; Hakala, J.; Donahue, N. M.; Robinson, E. S. Vapor Wall Loss of Semi-Volatile Organic Compounds in a Teflon Chamber. *Aerosol Sci. Technol.* **2016**, *50*, 822–834.
- (46) Reid, J. P.; Bertram, A. K.; Topping, D. O.; Laskin, A.; Martin, S. T.; Petters, M. D.; Pope, F. D.; Rovelli, G. The Viscosity of Atmospherically Relevant Organic Particles. *Nat. Commun.* **2018**, *9*, 1–14.